

Spatial heterogeneity of T cell repertoire across NSCLC tumors, tumor edges, adjacent and distant lung tissues

Qikang Hu^{a,b,c#}, Meredith L. Frank^{d#}, Yang Gao^{e,f,g,h#}, Liyan Ji, Muyun Peng^{a,b,c}, Chen Chen^{a,b,c}, Bin Wang^{a,b,c}, Yan Hu^{a,b,c}, Zeyu Wu^{a,b,c}, Jina Li^{a,b,c}, Lu Shu^{a,b,c}, Qiongzi Heⁱ, Yingqian Zhangⁱ, Xuefeng Xiaⁱ, Jianjun Zhang^{d,j,k,l}, Xin Yiⁱ, Alexandre Reuben^m, and Fenglei Yu^{a,b,c}

^aDepartment of Thoracic Surgery, The Second Xiangya Hospital of Central South University, Changsha, P. R. China; ^bHunan Key Laboratory of Early Diagnosis and Precise Treatment of Lung Cancer, The Second Xiangya Hospital of Central South University, Changsha, China; ^cEarly-Stage Lung Cancer Center, The Second Xiangya Hospital of Central South University, Changsha, China; ^dDepartment of Thoracic/Head and Neck Medical Oncology, University of Texas MD Anderson Cancer Center, Houston, USA; ^eDepartment of Thoracic Surgery, Xiangya Hospital, Central South University, Changsha, P. R. China; ^fXiangya Lung Cancer Center, Xiangya Hospital, Central South University, Changsha, China; ^gHunan Engineering Research Center for Pulmonary Nodules Precise Diagnosis & Treatment, Changsha, China; ^hNational Clinical Research Center for Geriatric Disorders, Changsha, China; ⁱGeneplus-Beijing Institute, Beijing, China; ^jDepartment of Genomic Medicine, University of Texas MD Anderson Cancer Center, Houston, USA; ^kLung Cancer Genomics Program, University of Texas MD Anderson Cancer Center, Houston, USA; ^lLung Cancer Interception Program, University of Texas MD Anderson Cancer Center, Houston, USA

ABSTRACT

Background: A better understanding of T cells in lung cancer and their distribution across tumor-adjacent lungs and peripheral blood is needed to improve efficacy and minimize toxicity from immunotherapy to lung cancer patients.

Methods: Here, we performed CDR3 β TCR sequencing of 136 samples from 20 patients with early-stage NSCLC including peripheral blood mononuclear cells, tumors, tumor edges (<1 cm from tumor), as well as adjacent lungs 1 cm, 2 cm, 5 cm, and 10 cm away from the tumor to gain insight into the spatial heterogeneity of T cells across the lungs in patients with NSCLC. PD-L1, CD4, and CD8 expression was assessed using immunohistochemical staining, and genomic features were derived by targeted sequencing of 1,021 cancer-related genes. Multiplex immunohistochemistry against PD-1, CTLA4, LAG3, and TIM3 was performed on four patients to assess T cell exhaustion.

Results: Our study reveals a decreasing gradient in TIL Tumor Infiltrating Lymphocytes homology with tumor edge, adjacent lungs, and peripheral blood but no discernible distance-associated patterns of T cell trafficking within the adjacent lung itself. Furthermore, we show a decrease in pathogen-specific TCRs in regions with high T cell clonality and PD-L1 expression.

Conclusions: Exclusion in T exhaustion cells at play across the lungs of patients with NSCLC may potentially be the mechanism for lung cancer occurrence.

SUMMARY

What is already known on this topic – The immunomodulatory effects of the tumor microenvironment (TME) significantly impact the T cell repertoire resulting in different anti-tumor immune responses. Previous work by our group and others has highlighted intratumor heterogeneity in T cell clonality, spatial distribution, and diversity, as well as infiltration of bystander, and exhausted T cells in early-stage non-small-cell lung cancer (NSCLC). However, little is known about how TME impacts the T cell repertoire in distant or surrounding adjacent uninvolved lung tissue.

What this study adds – We used a step-wise approach to deconstruct the T cell repertoire architecture across six regions within NSCLC tumor tissue and the surrounding healthy lung tissue. T cell markers and repertoire metrics were compared across resected tissue from the tumor, tumor edge (<1 cm from tumor), and 1, 2, 5, and 10 cm away from the tumor across 20 lung adenocarcinoma patients in order to better understand the impact of the tumor on the T cell repertoire across the lungs.

How this study might affect research, practice, or policy – We found that the regions with the highest clonality also present the lowest number of predicted pathogen-specific TCRs. This lack of predicted pathogen-specific TCRs could suggest a higher probability of infiltration with tumor-specific TCRs. This study indicates that exclusion in T cells at play across the lungs of patients with NSCLC may be potentially the mechanism for lung cancer occurrence.

ARTICLE HISTORY







Received 3 November 2022

Revised 25 June 2023


Accepted 2 July 2023

KEYWORDS

IHC; NSCLC; T cell repertoire

CONTACT Xin Yi  yix@geneplus.org.cn  Geneplus-Beijing Institute, No. 6 Building, Peking University Medical Industrial Park, Changping District, Beijing, P. R. China; Alexandre Reuben  AREuben@mdanderson.org  Department of Thoracic/Head and Neck Medical Oncology, University of Texas MD Anderson Cancer Center, 1515 Holcombe Blvd, Houston, USA; Fenglei Yu  yufenglei@csu.edu.cn  Department of Thoracic Surgery, The Second Xiangya Hospital of Central South University, No 139 Renmin Middle Road, Changsha, Hunan, P. R. China

[#]This are co Author

 Supplemental data for this article can be accessed online at <https://doi.org/10.1080/2162402X.2023.2233399>

© 2023 The Author(s). Published with license by Taylor & Francis Group, LLC.

This is an Open Access article distributed under the terms of the Creative Commons Attribution-NonCommercial License (<http://creativecommons.org/licenses/by-nc/4.0/>), which permits unrestricted non-commercial use, distribution, and reproduction in any medium, provided the original work is properly cited. The terms on which this article has been published allow the posting of the Accepted Manuscript in a repository by the author(s) or with their consent.

Introduction

Lung cancer is the leading cause of cancer-related deaths and is expected to claim over 130,000 lives in the USA in 2022 alone^{1,2}. About 85% of lung cancer diagnoses are classified as non-small cell lung cancer (NSCLC)^{1,3}. While treatments for early-stage NSCLC bode decent success rates, 75% of patients present with late-stage diseases at the time of diagnosis, for which survival rates are poor^{3,4}. Immunotherapies, such as immune checkpoint blockade (ICB) or adoptive cell therapy (ACT) using autologous T cells, have led to substantial clinical benefits, yet a majority of patients do not respond to treatment or develop secondary resistance^{5,6}. On the other hand, although it is overall better tolerated than conventional chemotherapy, ICB can lead to serious toxicities, some of which can be lethal. These have prompted exploration into immune-related drivers of suboptimal responses and toxicities to identify biomarkers to stratify patients for more personalized treatments.

PD-L1 is a widely used predictive marker. However, application across large patient datasets has resulted in inconsistent predictive power⁷. Tumor mutational burden (TMB) is another biomarker associated with efficacious responses to ICB and adoptive transfer of expanded autologous CD8⁺ T cells^{8,9}. NSCLC tumors with higher TMBs generally have better clinical responses to ICB, perhaps due to a larger pool of neoantigen targets for CD8⁺ T cell recognition^{7,10–12}.

CD8⁺ T cells are critical mediators of anti-tumor responses as multiple groups have shown that higher numbers of CD8⁺ tumor infiltrating lymphocytes (TIL) are associated with improved outcomes^{13,14}. More specifically, recent work from our group identified intratumor differences in the T cell repertoire as prognostic tools in NSCLC. Multi-region TCR sequencing revealed that greater TCR ITH was associated with greater risk of relapse and higher intratumor ITH in clonality was associated with more aggressive disease progression and greater risk of relapse⁵. Our more recent work demonstrated that a high proportion of TCR overlaps between the tumor and adjacent healthy lung tissue and greater TCR overlap was associated with worse survival¹⁵. In these studies, we determined that by analyzing the homology in T cell repertoire between tumors and their adjacent lungs, we could identify T cells more likely to recognize viral antigens (bystander T cells), and that these bystander T cells were associated with worse outcomes. However, in our prior studies, we were not able to assess any spatial differences in the T cell repertoire of tumor-adjacent lungs based on proximity to the tumor¹⁵. Here, we used a step-wise approach to deconstruct the T cell repertoire architecture across six regions within NSCLC tumor tissue and the surrounding normal lung tissue. T cell markers and repertoire metrics were compared across resected tissue from the tumor, tumor edge (<1 cm from tumor), and 1, 2, 5, and 10 cm away from the tumor across 20 lung adenocarcinoma patients in order to better understand the impact of the tumor on the T cell repertoire across the lungs.

Materials and methods

Tissue collection

Tissue samples from a total of 20 patients with primary lung cancer were collected at Second Xiangya Hospital of Central South University from September to December 2018. All patients gave written informed consent. The study was approved by the Ethics Committee of Second Xiangya Hospital Central South University (IRB: 2020084). Tissues from tumor, tumor edge (defined as <1 cm away from tumor), 1 cm away from tumor, 2 cm away from tumor, 5 cm away from tumor, and 10 cm away from tumor were collected for each patient during resection. The FFPE blocks were split into two parts, one for H&E staining and another for IHC staining. Pathological assessment by H&E of tumor and tumor edges is shown in **Supplementary Fig. S1**.

Targeted sequencing

DNA was extracted from FFPE of tumor tissues using Promega Maxwell™ RSC DNA FFPE Kit (Lot: AS1135#847221). Blood DNA was used as control. One tumor that had insufficient DNA was excluded from sequencing. DNA (0.8–1.0 µg) was sheared into fragments with a peak of 200–250 bp for library preparation using NEBNext® Ultra™ DNA Library Prep Kit (NEB, Ipswich, MA). The barcoded libraries were captured by a customized panel of 1021 genes as previously described¹⁶. Sequencing was performed on a GeneSeq2000 (Suzhou GenePlus Clinical Laboratory Co., Suzhou, China) platform. Reads with low-quality [(a) read with a half bases with quality ≤5; (b) reads with N base ≥5%; (c) reads with average base quality <0] were removed from raw sequencing data. Then, clean reads were mapped into hg19 human genome using bwa, and reads were further analyzed through sentieon pipeline. Somatic single nucleotide variations and small indels were called by MuTect2 and TNScope, respectively. The SNVs were filtered using SNP databases including dbSNPs138, 1000 G, HAPMAP. Final SNVs and indels were filtered by variant allele frequency ≥1%. And the variant classifications were kept if they fell into the following categories: “Missense_Mutation”, “Frame_Shift_Ins”, “Frame_Shift_Del”, “Nonsense_Mutation”, “In_Frame_Ins”, “Splice_Site”, “In_Frame_Del”, “Non stop_Mutation”, and “Translation_Start_Site”.

T cell receptor sequencing

Sequencing for human TCRβ chain complementarities determining region 3 (CDR3) was performed as previously described¹⁷. Briefly, V and J genes of CDR3 gDNA were amplified with multi-plex primers. The PCR products were sequenced after fragment selection by Illumina platform with paired-end 100 bp. The clean data were obtained by removal of low-quality reads. Paired-end reads were used for MIXCR to map into V and J genes and annotated using the ImMunoGeneTics (IMGT) database. Pathogen associated TCRs were clustered with GLIPH2¹⁸ using pathogen-related Mc-PAS dataset.

Immunohistochemistry

PD-L1 was stained by PD-L1 (SP263) antibody (Roche) for tumor tissue, tumor edge, 1 cm, 2 cm, 5 cm, and 10 cm. Experiments were performed as manufacturer's instruction. Positive PD-L1 staining defined as (1) >25% of tumor cells exhibit positive membrane staining; (2) immune cells present (ICP) >1% and IC positive \geq 25%; or (3) ICP = 1% and IC⁺ = 100%. The IHC results for PD-L1 were viewed by two independent pathologists and averaged together for analysis. CD4 and CD8 antibodies were provided by Servicebio Inc (Wuhan, China) for tumor edges of 1 cm, 2 cm, 5 cm, and 10 cm from four patients. Immunohistochemistry score of CD4 and CD8 positive staining were quantified by artificial intelligence-assisted IHC scoring system (Servicebio Inc, Wuhan, China).

Multiplex immunohistochemistry staining on PD-1 (Abcarta, PA153), CTLA4 (Abcam, ab273048), LAG3 (ABGENT, AP6987c), and TIM3 (Abcarta, PA366) for tissues from tumors, tumor edge, 1 cm, 2 cm, 5 cm, 10 cm away from tumors. CKpan and DAPI were used for the identification of epithelial cells and total cells, respectively. Briefly, the FFPE slides were sequentially incubated with antibodies according to the manufacturer's instructions. And the positive staining was scanned by HITRAI Scanner and quantified by the HALO image analysis platform (Indica Labs, Scotland, UK).

Statistical analysis

All the statistics and graphs were analyzed by R (v 4.1.0). The Mann-Whitney U-test or t-test was used to determine the differences of numerous continuous data between groups.

Correlation was performed by Pearson coefficient. Paired t-tests and 2-way ANOVA were used when appropriate. Significant differences were considered if $p < 0.05$ with Holm's method for multiple comparison using default parameters of ggpubr package.

Results

Study design and patient cohort

To investigate the spatial T cell composition of the tumor and adjacent lung microenvironments, we enrolled a cohort of 20 patients with primary lung tumors (Figure 1A–B). Patients had early-stage (stage I-III) NSCLC and underwent lobectomies for curative intent (Supplementary table S1). Targeted sequencing was performed to evaluate the genomic landscape and revealed a high prevalence of *TP53* mutations (58%, 11/19 patients), *EGFR* mutations (47%, 9/19 patients), and *ZFH3* (21%, 4/19 patients) among others (Figure 1C). No difference in TCR repertoire was observed based on mutational landscape nor smoking status (Supplementary Fig. S2–3). TCR clonality and diversity were compared across all tissues for smokers versus nonsmokers with no differences seen between the two groups across all tissue samples, except 1 cm away from tumor (Supplementary Fig. S3A–3B). Interestingly, a higher TCR diversity was observed in well-differentiated tumor tissues at 10 cm adjacent normal, compared with moderately differentiated tumors ($p = 0.038$; Supplementary Fig. S3C). And a similar trend of TCR clonality was also observed in the blood ($p = 0.07$; Supplementary Fig. S3D), suggesting a potential T cell exchange between the adjacent tissue and blood.

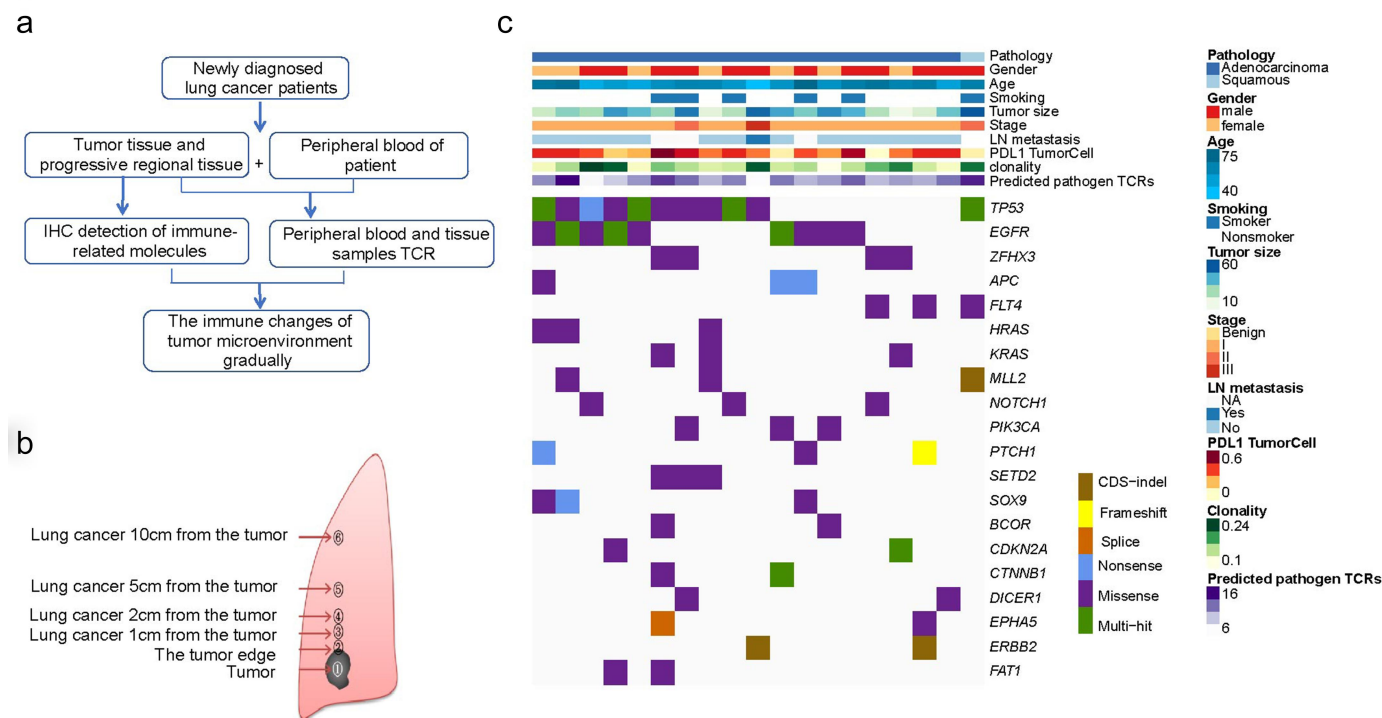


Figure 1. The workflow and mutational landscape. a: Schematic representation of experiment design. b: Tissue samples from a total of 6 regions were analyzed for TCR repertoire metrics across $n = 20$ NSCLC patients. c: Heatmap of clinical characteristics and tumor mutational data of top 20 mutated genes across ($n = 19$) patients.

Increasing gradient of CD8⁺ and PD-L1⁺ observed in tumor periphery

Previous studies on NSCLC have demonstrated that greater CD8⁺ T cell densities within the tumor and tumor edges are associated with increased overall survival and, conversely, higher CD4⁺ T cell densities are associated with worsened survival^{13,14}. Accordingly, we assessed changes in CD8⁺ and CD4⁺ T cell densities within tumor tissue and peripheral regions using immunohistochemistry (Figure 2A and Supplementary Fig. S4). No significant difference in CD8⁺ or CD4⁺ T cell densities was observed between tumor tissue and peripheral regions (Figure 2B–E). However, the CD8⁺:CD4⁺ ratio was higher in the tumor edge, when compared with the tumor itself, indicating the presence of CD8⁺-rich regions in the tumor periphery (Figure 2F). PD-L1 expression was also measured by immunohistochemistry but revealed no differences between regions (Supplementary Fig. S5). However, overall tumor peripheral regions exhibited higher PD-L1 expression on immune cells when compared to the tumor itself (Fig. S2A, 2 G–H).

Increasing gradient of exhausted T cells observed in tumor periphery

Exhausted T cells in the tumor microenvironment have been associated with cancer immune escape¹⁹. We further examined the infiltration of exhausted T cells by staining classic exhaustion markers including TIM3, PD1, LAG3, and CTLA4 in tumor and adjacent normal tissues (Figure 2I and Supplementary Fig. S6A). CKpan was used to distinguish tumoral and stromal regions (Supplementary Fig. S6A). PD1⁺, LAG3⁺, and TIM3⁺ cell densities increased from tumor cores to adjacent normal tissues, with a significant increase at 5 cm (all $p < 0.05$) (Supplementary Fig. S6B). Furthermore, co-expression of TIM3⁺PD1⁺LAG3⁺ was notably higher at 5 cm, compared to tumor. Furthermore, the percentage of TIM3⁺ and CTLA4⁺ cells were higher in tumoral regions (CKpan⁺) than in stromal regions (CKpan⁻) ($p = 0.029$ and $p = 0.029$, respectively), while PD1 showed no difference (Supplementary Fig. S6C).

Regions of T cell high diversity exhibited lowest clonality and PD-L1 expression

To assess the spatial distribution of T cell repertoire, we performed sequencing of the CDR3 β region of the T cell receptor primarily involved in antigen binding and analyzed related TCR metrics, namely, clonality and diversity. Clonality was calculated across regions for 21 patients (Figure 3A). Tumor tissue exhibited the lowest level of clonality but the highest level of diversity, whereas peripheral regions, namely 2 cm ($p = 8.3 \times 10^{-7}$), contained higher clonality but lower amounts of diversity, consistent with prior studies by our group¹⁵ and suggestive of a suppressed T cell repertoire within the tumor microenvironment ($p < 0.05$) (Figure 3B,C). No significance was found among the histological subtypes of lung adenocarcinoma (Supplementary Fig. S7A). PD-L1 expression was moderately associated

with clonality ($\rho = 0.407$, $p = 0.0487$) (Figure 3D), typically a trend at 10 cm away from the tumor ($R = 0.95$, $p = 0.051$) (Supplementary Fig. S7B). No significant correlation was observed between clonality and CD8⁺ density across all tissues (Supplementary Fig. S7C). The infiltration of TIM3⁺PD1⁺LAG3⁺ cells was strongly correlated with clonality in the tumor (Figure 3E), but not at tumor edges (Supplementary Fig. S7D).

Dominant T cell populations are better conserved in tumor margins compared to inside the tumors

Morisita overlap index (MOI) values were calculated between all available regions for 20 patients. As shown in Supplementary Fig. S8, substantial interpatient heterogeneity was observed among samples. As expected, a lower amount of overlap was seen between tumor tissue and all other tissues, with a modest overlap only with the tumor edge (Figure 3F) (MOI = 0.35). Most patients exhibited the highest overlap between 2 cm and surrounding regions, namely 5 cm, 1 cm, and the tumor edge (Figure 3F) (MOI = 0.57, 0.56, and 0.58, respectively). In general, dominant T cell populations were better conserved between the tumor margins and “hot regions” of increased clonality compared to the tumors (Figure 3F).

High clonality regions are infiltrated by fewer predicted pathogen-specific T cells

As large numbers of bystander T cells in tumor tissue have been identified in NSCLC and other solid tumors^{15,20,21}, we next analyzed the pathogen specificity within tissue regions. GLIPH analysis was used to cluster similar CDR3 motifs which were cross-referenced against publicly available viral CDR3 motifs to predict viral antigen specificity. Predicted pathogen TCR counts were calculated for all regions across 20 patients (Figure 4A). Pathogen-specific TCR counts varied significantly between regions with tumor tissue containing the highest proportion of pathogen-specific TCRs (Figure 4B). Clonality was inversely proportional to pathogen count ($R = -0.3$, $p = 0.00094$, Figure 4C and Supplementary Fig. S9). Interestingly, the tumor contained the highest clonality and also exhibited a strong positive association between the amount of predicted pathogen TCRs and CD8⁺ density ($R = 0.99$, $p = 0.0092$), but not CD4⁺ cell density ($R = 0.4$, $p = 0.6$), potentially suggesting preferential expansion of non-viral CD8⁺ T cells in tumor (Supplementary Fig. S10A–B). In tumor tissue, no correlation was observed between CD4⁺ T cell density and the amount of predicted pathogen TCRs (Figure 4D). In tumor tissues, the amount of pathogen-specific TCRs negatively correlated with TCR clonality (Figure 4E) but positively with CD8⁺ T cell density (Figure 4F), indicating the presence, but lack of expansion, of pathogen-specific T cells within the tumor (Figure 4F). A moderate, but statistically significant, association was observed between the proportion of predicted pathogen TCRs and tumor cell PD-L1 expression ($R = 0.46$, $p = 0.044$) (Figure 4G). Pathogen-specific TCR counts positively associated with TIM3⁺PD1⁺LAG3⁺ infiltration ($R = 0.6$, $p = 0.0019$) (Figure 4H).

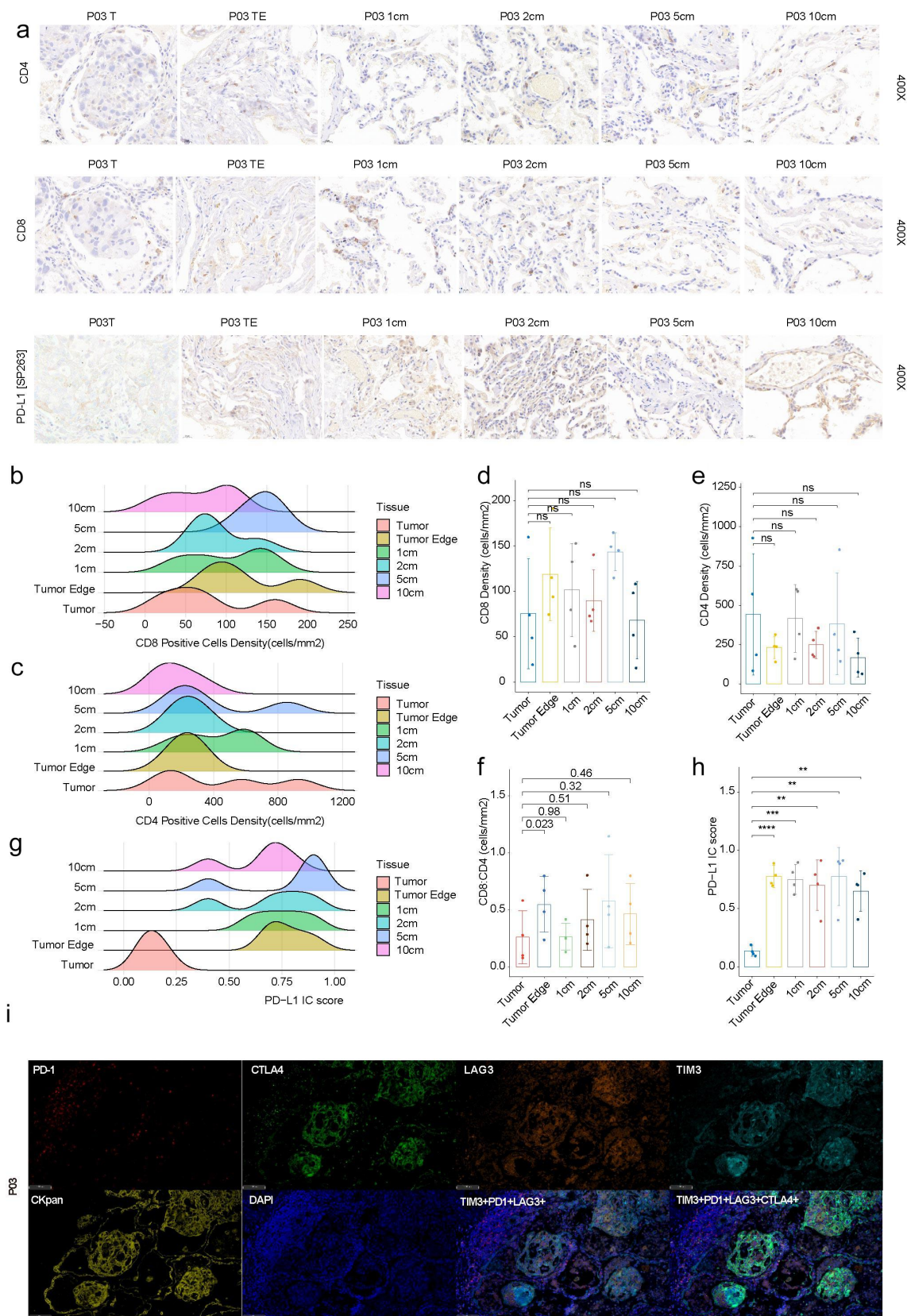


Figure 2. Immunohistochemistry on T cell markers in tumor, tumor edge, 1 cm, 2 cm, 5 cm, and 10 cm adjacent normal tissues of early NSCLC patients. **a:** the representative images of immunohistochemical staining on CD4, CD8, and PD-L1 in tumor, tumor edge, 1 cm, 2 cm, 5 cm, and 10 cm adjacent normal tissues. **b:** CD8+ cell density (cells/mm²) measured by IHC across all tissues for $n = 4$ patients. **c:** CD4+ cell density (cells/mm²) measured by IHC across all tissues for $n = 4$ patients. **d:** Boxplot represents the comparison of CD8+ cell density across all tissues. Mann-Whitney U-test was used for statistical analysis. **e:** Boxplot represents the comparison of CD4+ cell density across all tissues. Mann-Whitney U-test was used for statistical analysis. **f:** Median CD8+ and CD4+ cell densities (cells/mm²) across all regions for $n = 4$ patients. **g:** PD-L1 score measured by IHC across all tissues for $n = 4$ patients. **h:** Boxplot represents the comparison of PD-L1 score across all tissues. Mann-Whitney U-test was used for statistical analysis. **i:** the representative images of multiplex immunohistochemistry show the expression of CKpan, TIM3, PD1, LAG3, and CTLA4 in tumor, tumor edge, and 1 cm, 2 cm, 5 cm, and 10 cm adjacent normal tissues. Scale bar, 100 μ m.

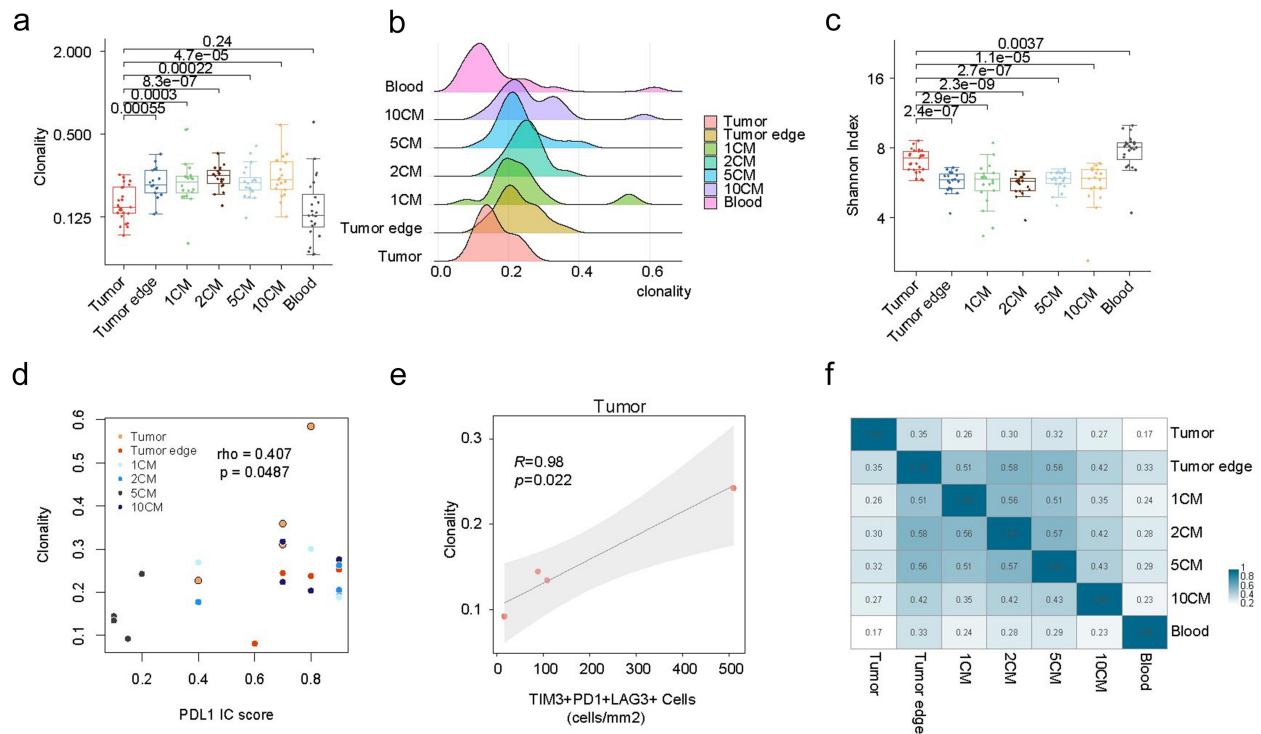


Figure 3. The TCRs features in tumor, tumor edge, 1 cm, 2 cm, 5 cm, and 10 cm adjacent normal tissues of early NSCLC patients. a: Clonality values for all samples for $n = 20$ patients. b: Median clonality across regions for $n = 20$ patients. c: Median Shannon index values across regions for $n = 20$ patients. d: Clonality versus PD-L1 expression (all tissues combined). Pearson's coefficient was used to analyze the association between clonality and PD-L1 expression across all tissues for $n = 4$ patients. e: Clonality versus TIM3⁺PD1⁺LAG3⁺ cell infiltration in tumor ($n = 4$). f: Average morisita overlap between regions for $n = 20$ patients. From top to bottom: tumor, tumor edge, 1 cm, 2 cm, 5 cm, 10 cm from tumor, peripheral blood, respectively. From left to right: tumor, tumor edge, 1 cm, 2 cm, 5 cm, 10 cm from tumor, peripheral blood.

Discussion

Checkpoint blockade immunotherapy reactivates T cells exhibiting a given phenotype at the systemic level, regardless of antigen-specificity²². Considering that PD-1 is indiscriminately expressed on T cells following antigen exposure, reactivation of these T cells may be suboptimal²³. Thus, a better understanding of the T cell repertoire and immune microenvironment in the context of the lungs is needed. Here, we performed TCR sequencing on a series of matched samples from 20 patients with early-stage NSCLC. To assess T cell infiltration across the lungs, we obtained samples from tumors, tumor edges, as well as 1 cm, 2 cm, 5 cm, and 10 cm stepping away from the tumor in addition to from matched peripheral blood.

Our spatial analysis of T cell infiltration allowed us to assess spatial T cell distribution across the lungs. Although tumors and adjacent lungs have previously been compared by us and others, such a dissection of the lung spatial environment and its T cell infiltrate and repertoire has not yet been undertaken¹⁵. Analysis of the homology in the T cell repertoire between the tumor and adjacent lung regions proved consistent with our prior findings. Indeed, the MOI between the tumor and adjacent lung was ~ 0.28 , consistent with a prior study by our group demonstrating a median of ~ 0.3 between tumors and adjacent lungs¹⁵. The same could be said for MOI between the tumor and peripheral blood, which was ~ 0.18 in our study and ~ 0.15 in the same prior study¹⁵. However, an important dimension not captured in our prior study was the inclusion of the tumor edge, which showed the highest homology with the tumor, highlighting the overall decrease in gradient in T cell homology

from the tumor edge (MOI = 0.36), to adjacent lung (0.28), and peripheral blood (0.18). The MOI between tumor and tumor edge was also below what was observed in our prior analysis of intratumor heterogeneity (MOI = 0.85), as should be expected⁵. As an extension of our previous studies, we further observed the heterogeneity between stromal and intra-tumoral TILs, specifically, exhausted T cells, as well as the spatial tumor microenvironment heterogeneity at step-wise distribution from tumor core to tumor edges tumor adjacent to normal lung tissues. The lower homology between the tumor and all regions of the adjacent lungs is suggestive of the potential presence of immune and T cell, especially exhausted T cell exclusion mechanisms within the tumor, which prevent T cell infiltration and could therefore explain the higher homology outside the tumor^{24,25}.

Our analysis revealed increased T cell diversity and decreased T cell clonality in the tumor compared to the tumor edge and adjacent lungs. This supports prior studies by our group in larger cohorts with a lower spatial resolution¹⁵. Interestingly, by using GLIPH2.0¹⁸, we demonstrate that regions with the highest clonality also present the lowest number of predicted pathogen-specific TCRs. This lack of predicted pathogen-specific TCRs could suggest a higher probability of infiltration with tumor-specific TCRs. Although this could be influenced by the increased diversity in pathogen TCR-rich regions, positive correlation between PD-L1 and T cell clonality might be suggestive of adaptive resistance induced by T cell activation and IFN- γ secretion, further supporting our hypothesis.

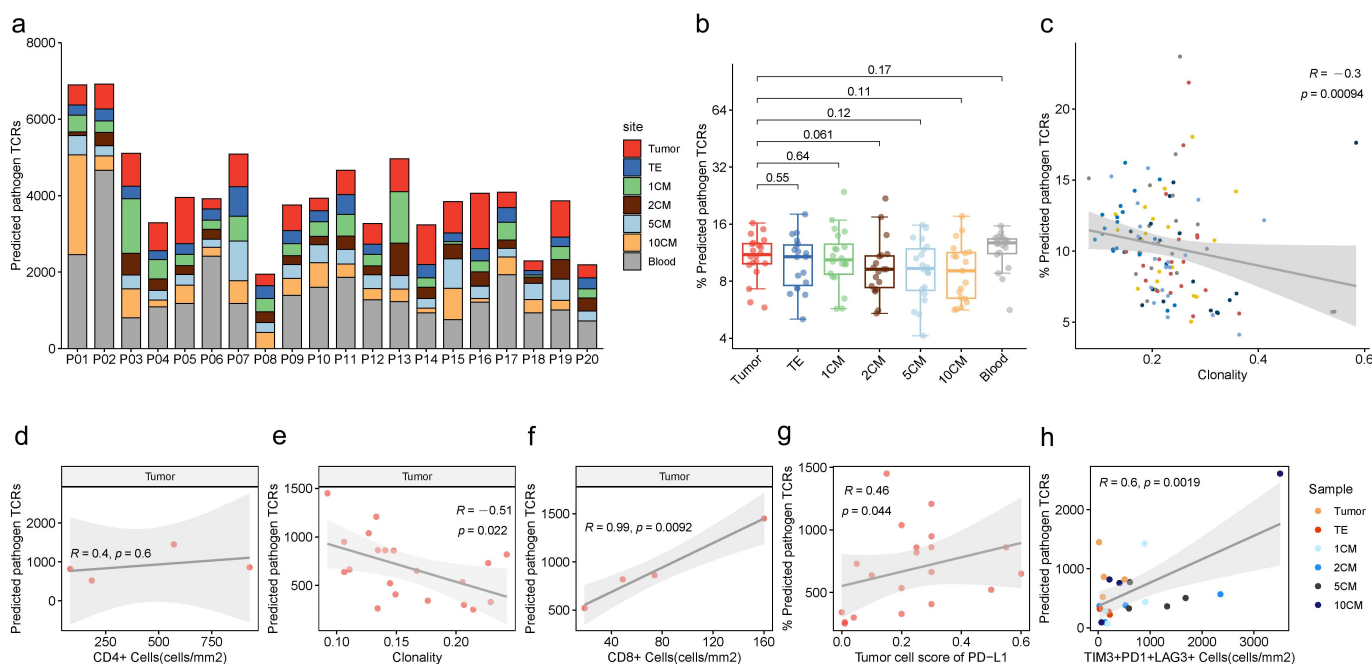


Figure 4. The predicted pathogen associated TCRs in tumor, tumor edge, 1 cm, 2 cm, 5 cm, and 10 cm adjacent normal tissues of early NSCLC patients. a: Percentage of predicted pathogen TCRs across all regions for $n = 20$ patients. b: Median percentage of predicted pathogen TCRs across all regions for $n = 20$ patients. c: Regional clonality values were plotted against median proportion of predicted pathogen TCRs for all tissues. The solid line represents correlation between clonality and predicted pathogen TCRs. Thin dotted lines represent the 95% confidence interval. d: Predicted pathogen TCRs (absolute count) versus CD4+ cell density (cells/mm²) for tumor tissue. Pearson's coefficient was used to analyze the association between the number of predicted pathogen specific TCRs and CD4+ cell density in tumor tissue for $n = 4$ patients. e: Predicted pathogen TCRs (absolute count) versus clonality for tumor tissue. Pearson's coefficient was used to analyze the association between the number of predicted pathogen-TCRs and clonality in tumor tissue for $n = 20$ patients. f: Predicted pathogen TCRs (absolute count) versus CD8+ cell density (cells/mm²) for tumor tissue. Pearson's coefficient was used to analyze the association between the number of predicted pathogen specific TCRs and CD8+ cell density in tumor tissue for $n = 4$ patients. g: PD-L1 score versus predicted pathogen-specific TCRs. Pearson's coefficient was used to analyze the association between PD-L1 score and predicted pathogen-specific TCRs in tumor tissue for $n = 20$ patients. h: The density of TIM3⁺PD1⁺LAG3⁺ cells versus predicted pathogen-specific TCRs. Pearson's coefficient was used to analyze the association between TIM3⁺PD1⁺LAG3⁺ cell infiltration and predicted pathogen specific TCRs across all tissues for $n = 4$ patients.

Our study does present certain limitations. First, despite our ability to reproduce several findings from prior studies, our study suffers from a limited sample size, which may have impaired our ability to attain statistical significance in certain settings. However, our analysis of 143 samples provides an unprecedented high-resolution analysis of the T cell repertoire in the lungs of NSCLC patients. Second, our analysis of immune phenotypes was unfortunately limited by a lack of tissue availability and a restriction to formalin-fixed paraffin-embedded tissues, preventing us from performing any deeper phenotyping and/or tying TCR sequence to phenotype as has recently been done by others using single-cell approaches²⁶. Third, our analysis of antigen-specificity via GLIPH2.0 remains predictive based on *in silico* analyses and will need to be validated with fresh samples via functional assays, although these were unfortunately unavailable in this context. Finally, our study is based on an Asian patient cohort with high frequency of EGFR mutant lung cancers, consistent with previous studies^{27–30}. Therefore, the findings in our study may not be applicable to Western patient population. Nonetheless, our study provides critical information as to the spatial CD4/CD8 T cell composition in the lungs, which has not been described by others to date. Overall, our study reveals the exclusion of T cells at play across the lungs of patients with NSCLC, as well as the unique T cell, PD-L1, and pathogen-specific T cell distribution patterns within these patients.

Acknowledgments

We thank SAN VALLEY DIAGNOSTICS, Servicebio Co., and Suzhou Abcarta Medical Technology Co. for their assistance with IHC experiments.

Disclosure statement

No potential conflict of interest was reported by the authors.

Funding

This work was supported by the National Natural Science Foundation of China (81972195 to Dr. Fenglei Yu), Hunan Provincial Key Area R&D Program (2019SK2253 to Dr. Fenglei Yu), and the National Clinical Key Specialty Construction Project (to Dr. Fenglei Yu). This investigation was also supported by the Natural Science Foundation of Hunan Province (2022JJ30925 to Yang Gao) and the Project Program of National Clinical Research Center for Geriatric Disorders (Xiangya Hospital, Grant No. 2021LNJJ17 to Yang Gao)

ORCID

Alexandre Reuben  <http://orcid.org/0000-0003-4510-0382>

Authors' contributions

Qikang Hu, Jianjun Zhang, Xuefeng Xia, Xin Yi, Alexandre Reuben and Fenglei Yu: conception and design, acquisition of data, data analysis and

interpretation, manuscript drafting, critical revision; statistical analyses. Meredith Frank, Liyan Ji, Qiongzhi He, Yingqian Zhang and Jianjun Zhang: manuscript drafting. Jianjun Zhang, Yin Yi, Alexandre Reuben and Fenglei Yu: conceived of the idea, supervised this project, and revised the manuscript. Meredith Frank, Liyan Ji, Qiongzhi He, Yingqian Zhang, Alexandre Reuben, Muyun Peng, Chen Chen and Xuefeng Xia: acquisition of data, data analysis, and interpretation. Qikang Hu, Meredith Frank, Yang Gao, Muyun Peng, Chen Chen, Liyan Ji: contributed reagents/materials/analysis tools. Fenglei Yu, Yang Gao: obtained funding.

Ethics approval and consent to participate

The study was approved by the Ethics Committee of Second Xiangya Hospital Central South University (IRB: 2020084).

Consent for publication

All authors have read and approved the article.

Availability of data and material

The authors declare that the data supporting the findings of this study are available within the paper and its Supplementary materials. All data generated during this study are included in this published article and its supplementary information files. All data in this study are available from the corresponding author with a reasonable request.

List of Abbreviations

ACT	adoptive cell therapy
CDR3	complementarities determining region 3
ICB	immune checkpoint blockade
ICP	immune cells present
IMGT	ImMunoGeneTics
MOI	Morisita overlap index
NSCLC	non-small cell lung cancer
TIL	tumor infiltrating lymphocytes
TMB	Tumor mutational burden

References

- Al-Shahrabani F, Vallbohmer D, Angenendt SKnoefel WT. Surgical strategies in the therapy of non-small cell lung cancer. *World J Clin Oncol.* 2014;5(4):595–603. doi:10.5306/wjco.v5.i4.595.
- American Cancer Society. (2022). Cancer facts & figures 2022. from <https://www.cancer.org/research/cancer-facts-statistics/all-cancer-facts-figures/cancer-facts-figures-2022.html>.
- Siegel R L, Miller K D, Fuchs H, E, Jemal A. Cancer Statistics, 2021. *CA Cancer J Clin.* 2021;71(1):7–33. doi:10.3322/caac.21654.
- Gadgeel SM, Ramalingam S, Skolemkerian GP. Treatment of lung cancer. *Radiologic Clinics of North America.* 2012;50(5):961–974. doi:10.1016/j.rcl.2012.06.003.
- Reuben A, Gittelman R, Gao J, Zhang J, Yusko EC, Wu C-J, Emerson R, Zhang J, Tipton C, Li J. TCR Repertoire Intratumor Heterogeneity in Localized Lung Adenocarcinomas: An Association with Predicted Neoantigen Heterogeneity and Postsurgical Recurrence. *Cancer Discov.* 2017;7(10):1088–1097. doi:10.1158/2159-8290.CD-17-0256.
- Creelan BC, Wang C, Teer JK, Toloza EM, Yao J, Kim S, Landin AM, Mullinax JE, Saller JJ, Saltos AN. Tumor-infiltrating lymphocyte treatment for anti-PD-1-resistant metastatic lung cancer: a phase I trial. *Nat Med.* 2021;27(8):1410–1418. doi:10.1038/s41591-021-01462-y.
- Jiang Z, Zhou YHuang Y, Huang J. A combination of biomarkers predict response to immune checkpoint blockade therapy in non-small cell lung cancer. *Front Immunol.* 2021;12:813331. doi:10.3389/fimmu.2021.813331.
- Lauss M, Donia M, Harbst K, Andersen R, Mitra S, Rosengren F, Salim M, Vallon-Christersson J, Törngren T, Kvist A. Mutational and putative neoantigen load predict clinical benefit of adoptive T cell therapy in melanoma. *Nat Commun.* 2017;8(1):1738. doi:10.1038/s41467-017-01460-0.
- Jardim DL, Goodman A, de Melo Gagliato DKurzrock D, Kurzrock R. The challenges of tumor mutational burden as an immunotherapy biomarker. *Cancer Cell.* 2021;39(2):154–173. doi:10.1016/j.ccell.2020.10.001.
- Rizvi H, Sanchez-Vega F, La K, Chatila W, Jonsson P, Halpenny D, Plodkowski A, Long N, Sauter JL, Rehkman N. Molecular determinants of response to anti-programmed cell death (PD)-1 and aNTI-PROGRAMMED DEATH-LIGAND 1 (PD-L1) blockade in patients with non-small-cell lung cancer profiled with targeted next-generation sequencing. *J Clin Oncol.* 2018;36(7):633–641. doi:10.1200/JCO.2017.75.3384.
- Buttner R, Longshore JW, Lopez-Rios F, Merkelbach-Bruse S, Normanno N, Rouleau E, Penault-Llorca F. Implementing TMB measurement in clinical practice: considerations on assay requirements. *ESMO Open.* 2019;4(1):e000442. doi:10.1136/esmoopen-2018-000442.
- High TMB predicts immunotherapy benefit. *Cancer Discov.* 2018;8(6):668. doi:10.1158/2159-8290.CD-NB2018-048.
- Kim SH, Go SI, Song DH, Park SW, Kim HR, Jang I, Kim JD, Lee JS, Lee G-W. Prognostic impact of CD8 and programmed death-ligand 1 expression in patients with resectable non-small cell lung cancer. *Br J Cancer.* 2019;120(5):547–554. doi:10.1038/s41416-019-0398-5.
- Feldmeyer L, W HC, Ray-Lyons G, Nagarajan P, Density APP, Curry JL, Torres-Cabala CA, Mino B, Rodriguez-Canales J, Reuben A. Distribution, and composition of immune infiltrates correlate with survival in Merkel cell carcinoma. *Clin Cancer Res.* 2016;22(22):5553–5563. doi:10.1158/1078-0432.CCR-16-0392.
- Reuben A, Zhang J, Chiou SH, Gittelman RM, Li J, Lee W-C, Fujimoto J, Behrens C, Liu X, Wang F. Comprehensive T cell repertoire characterization of non-small cell lung cancer. *Nat Commun.* 2020;11(1):603. doi:10.1038/s41467-019-14273-0.
- Tian P, Zeng H, Ji L, Ding Z, Ren L, Gao W, Fan Z, Li L, Le X, Li P. Lung adenocarcinoma with ERBB2 exon 20 insertions: Computations and immunogenomic features related to chemoimmunotherapy. *Lung Cancer.* 2021;160:50–58. doi:10.1016/j.lungcan.2021.07.014.
- Han J, Yu R, Duan J, Li J, Zhao W, Feng G, Bai H, Wang Y, Zhang X, Wan R. Weighting tumor-specific TCR repertoires as a classifier to stratify the immunotherapy delivery in non-small cell lung cancers. *Sci Adv.* 2021;7(21). doi:10.1126/sciadv.abd6971.
- Huang H, Wang C, Rubelt F, Scriba T, JDavis M M. Analyzing the Mycobacterium tuberculosis immune response by T-cell receptor clustering with GLIPH2 and genome-wide antigen screening. *Nat Biotechnol.* 2020;38(10):1194–1202. doi:10.1038/s41587-020-0505-4.
- Jiang Y, Li YZhu B, Zhu B. T-cell exhaustion in the tumor microenvironment. *Cell Death Disease.* 2015;6(6):e1792. doi:10.1038/cddis.2015.162.
- Simoni Y, Becht E, Fehlings M, Loh CY, Koo SL, Teng KWW, Yeong JPS, Nahar R, Zhang T, Kared H. Bystander CD8(+) T cells are abundant and phenotypically distinct in human tumour infiltrates. *Nature.* 2018;557(7706):575–579. doi:10.1038/s41586-018-0130-2.
- Scheper W, Kelderman S, Fanchi LF, Linnemann C, Bendle G, de Rooij MAJ, Hirt C, Mezzadra R, Slagter M, Dijkstra K. Low and variable tumor reactivity of the intratumoral TCR repertoire in human cancers. *Nat Med.* 2019;25(1):89–94. doi:10.1038/s41591-018-0266-5.
- Sharma PAllison JP, Allison JP. The future of immune checkpoint therapy. *Science.* 2015;348(6230):56–61. doi:10.1126/science.aaa8172.
- Granic C, De Guillebon E, Blanc C, Roussel H, Badoual C, Colin E, Saldmann A, Gey A, Oudard S, Tartour E. Mechanisms of action and

- rationale for the use of checkpoint inhibitors in cancer. *ESMO Open*. 2017;2(2):e000213. doi:10.1136/esmoopen-2017-000213.
24. Peranzoni E, Lemoine J, Vimeux L, Feuillet V, Barrin S, Kantari-Mimoun C, Bercovici N, Guérin M, Biton J, Ouakrim H. Macrophages impede CD8 T cells from reaching tumor cells and limit the efficacy of anti-PD-1 treatment. *Proc Natl Acad Sci U S A*. 2018;115(17):E4041–e4050. doi:10.1073/pnas.1720948115.
 25. Spranger S. Mechanisms of tumor escape in the context of the T-cell-inflamed and the non-T-cell-inflamed tumor microenvironment. *Int Immunol*. 2016;28(8):383–391. doi:10.1093/intimm/dxw014.
 26. Liu B, Hu X, Feng K, Gao R, Xue Z, Zhang S, Zhang Y, Corse E, Hu Y, Han W. Temporal single-cell tracing reveals clonal revival and expansion of precursor exhausted T cells during anti-PD-1 therapy in lung cancer. *Nat Cancer*. 2022;3(1):108–121. doi:10.1038/s43018-021-00292-8.
 27. Wang C, Yin R, Dai J, Gu Y, Cui S, Ma H, Zhang Z, Huang J, Qin N, Jiang T. Whole-genome sequencing reveals genomic signatures associated with the inflammatory microenvironments in Chinese NSCLC patients. *Nat Commun*. 2018;9(1):2054. doi:10.1038/s41467-018-04492-2.
 28. Hu X, Fujimoto J, Ying L, Fukuoka J, Ashizawa K, Sun W, Reuben A, Chow C-W, McGranahan N, Chen R. Multi-region exome sequencing reveals genomic evolution from preneoplasia to lung adenocarcinoma. *Nat Commun*. 2019;10(1):2978. doi:10.1038/s41467-019-10877-8.
 29. Jiang T, Shi J, Dong Z, Hou L, Zhao C, Li X, Mao B, Zhu W, Guo X, Zhang H. Genomic landscape and its correlations with tumor mutational burden, PD-L1 expression, and immune cells infiltration in Chinese lung squamous cell carcinoma. *J Hematol Oncol*. 2019;12(1):75. doi:10.1186/s13045-019-0762-1.
 30. Chen J, Yang H, Teo ASM, Amer LB, Sherbaf FG, Tan CQ, Alvarez JJS, Lu B, Lim JQ, Takano A. Genomic landscape of lung adenocarcinoma in East Asians. *Nat Genet*. 2020;52(2):177–186. doi:10.1038/s41588-019-0569-6.